JJMIE

Volume 18, Number 1, March. 2024
ISSN 1995-6665
Pages 15 - 30
https://doi.org/10.59038/jjmie/180102
Editor-in-Chief: Prof. Ali M. Jawarneh

Jordan Journal of Mechanical and Industrial Engineering

# A novel magnetohydrodynamic power generation system using low-temperature liquid metal coupled with a rectangular single-phase natural circulation loop

G. M. Tashtoush*, T. K. Aldoss, A. O. Al-Jabaly

*Jordan University of Science and Technology, Department of Mechanical Engineering, P.O.Box 3030, Irbid 22110, Jordan*

*Received 17 Jul 2023* *Accepted 17 Dec 2023*

**Abstract**

A 2D model of a rectangular single-phase natural circulation loop(SPNSL) with a magnetohydrodynamic power generator (MHDG) using low-temperature liquid metal (LM) as the working fluid is presented in this work. Two pairs of magnets were applied, one on the heater and another one on the cooler. The SPNCL is considered to dispense with the moving mechanical parts needed to drive the working flow through the system.Using Low-temperature liquid metal is considered cheap, easy to handle, low-grade heat sources, and low-cost permeant magnets. The parametric study was presented for the effect of Rayleigh number (Ra), Aspect ratio (Ar), and Hartmann number (Ha) on the Reynolds Number (Re), Nusselt Number (Nu) and generated electrical current, and power for Mercury as the working fluid,using numerical software. Furthermore, the comparison between Mercury and Gallium was presented. Verification results were presented in good agreement with the literature results. Moreover, the statistical analysis was investigated, using factorial analysis and the response surface method using statistical software for Ra, Ar, Ha, and type of liquid metal (TLM). The statistical results using the response surface method show fair agreement with the existing CFD results. The Re increases with the increase of the Ra and decreases with increasing the Ha and Ar. Increasing the Ar requires an increase in the Ra and Ha to obtain the maximum electrical power. By comparing the performance of Mercury with Gallium, Gallium generated more electrical power than Mercury.



**Keywords:** Magnetohydrodynamic generator, Natural flow circulation, Low-temperature liquid metal, Computational fluid dynamics, Statistical Analysis.

## Nomenclature

| | |
|---|---|
| MHDG | Magnetohydrodynamic Power Generator |
| MHD | Magnetohydrodynamic |
| NCL | Natural Circulation Loop |
| SPNCL | Single-Phase Natural Circulation Loop |
| LM | Liquid Metal |
| DoE | Design of Experiments |
| ANOVA | Analysis of Variance |
| RSM | Response Surface Methodology |
| CFD | Computational Fluids Dynamics |
| TLM | Type of Liquid Metal |
| μ | Dynamic Viscosity [Kg/m.s] |
| $\nu$ | Kinematic Viscosity [$m^2/s$] |
| ρ | Density [Kg/ $m^3$] |
| $C_p$ | Specific Heat at Constant Pressure [J/Kg.K] |
| β | Coefficient of Thermal Expansion [1/K] |
| K | Thermal Conductivity [W/m.K] |
| σ | Electrical conductivity [siemens/m] |
| h | heat transfer coefficient [W/ $m^2$.K] |
| Pr | Prandtl Number |
| Re | Reynolds Number |
| Ra | Rayleigh Number |
| Ha | Hartmann Number |
| Ar | Aspect Ratio |
| L | Length [m] |
| W | Width [m] |
| $D_h$ | Hydraulic Diameter |
| H | Height of the Heater/Cooler |
| N | North |
| S | South |
| + | High |
| - | Low |
| V | Dimensionless Vertical Velocity |
| U | Dimensionless Horizontal Velocity |
| $\alpha$ | Thermal Diffusivity [$m^2/s$] |
| P | Dimensionless pressure |
| $\theta$ | Dimensionless Temperature |
| Ec | Eckert Number |
| Nu | Nusselt Number |
| $B$ | Magnetic Field [Tesla] |
| g | Gravitational Acceleration [m/ $s^2$] |
| J | Current Density [A/ $m^2$] |
| W | Electrical Power [W] |

**Superscript**

| | |
|---|---|
| * | Dimensionless Form |

**Subscripts**

| | |
|---|---|
| o | Reference |
| ex | External |
| O | Outer |
| i | Inner |
| h | Heater |
| c | Cooler |
| Avg | Average |

* Corresponding author e-mail: gtash@just.edu.jo.

  - Volume 18, Number 1 (ISSN 1995-6665)

## 1. Introduction

A magnetohydrodynamic power generator (MHDG) is a device used to convert mechanical energy into electrical energy with no moving mechanical parts. Magnetohydrodynamic (MHD) power generation involves many applications in recent technology and industry, like that found in electrical power plants (thermal or nuclear plants). Direct power generation uses the available heat sources including waste heat, solar energy, and other renewable energies.Moreover, MHDG becomes more economically competitive when combined with certain applications such as solar and nuclear energy conversion[1].

One of the advantages of the MHDG is the ability to use a natural circulation loop (NCL) that dispense with the moving mechanical parts. Dispense with mechanical devices has several advantages, such as reducing mechanical losses, being of less operational cost and a more reliable system that has a modular structure. MHD power plants that use very high-temperature gases proved to have higher efficiency than conventional power plants especially when super magnetization is used. One major element of the MHDG is the electrically conducting fluids, such as plasmas (very hot gasses), liquid metals, and saltwater.

In general, the MHDG and the single-phase natural circulation loop (SPNCL) have captured the interest of many researchers in recent years. The published studies can be categorized into three categories, experimental, numerical, and analytical. Different working fluids were considered. Applications can be divided into very high-grade energy sources like the one found in nuclear power plants, low-grade energy sources found as waste heat in different industries, energy harvested from solar, and other renewable energy sources.

### *1.1. Magnetohydrodynamic Power Generator (MHDG)*

The principle of MHDG is governed by Faraday's law of induction. The basic construction of MHDG is shown in **Figure 1.a** where the electrically conducting fluid flows through a magnetic field where an electric field is generated and picked up using the electrodes (anode and cathode), The magnetic field must be perpendicular to the direction of the flow and the electric field.

Experimental, numerical, and theoretical studies of MHDGs using liquid metal and salt water as the working fluids with different heat sources have been conducted by different researchers [2-23]. Experimental and mathematical 3D Multiphysics model investigation of MHDG with a low-temperature liquid metal using pure Gallium as the working fluid was studied by Cosoroaba et al. [2]. Their mathematical model of MHDG is built in COMSOL Multiphysics software. They claimed a good agreement between the simulation and the experiment, and stated that pure Gallium has better electrical conductivity, than lead, Galinstan, PbLi, and GaInSn. Niu et al. [3] investigated MHDG using a low melting point Gallium alloy with a uniform magnetic field at high Reynolds number experimentally and theoretically. They concluded that the maximum power generation efficiency was 8.3E-04 % and the maximum output electric power of 1.5 mW based on the non-uniform distribution of the magnetic field in the test channel. The hydrodynamic and thermal behavior of parallel vertical plates with MHD was studied byHamdan et al.[4]. They found that the skin friction factor, Nusselt (Nu) number and the thickness of the velocity boundary layer decreased with the increasing of the magnetic field Kn number. Where the magnetic field caused an increase in the fluid temperature. The fully developed natural convection MHD micropolar fluid flow in a vertical channel was analyzed by Malga et al. [5]. They solved the coupled non-linear governing equations by the finite element method. They found that the effects of viscous dissipation are significant, where the increase in the velocity increases the viscous dissipation parameter (Ec).

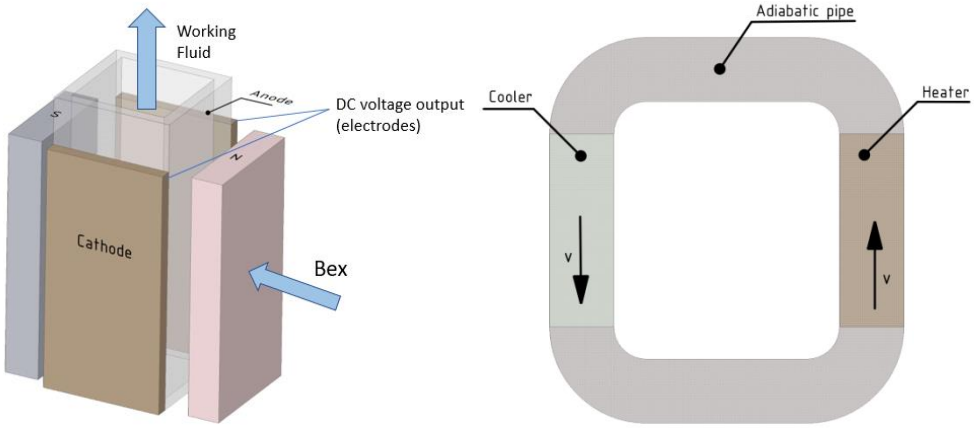


a.) MHDG b.) SPNCL

**Figure 1.** Schematic Diagram of MHDG and SPNCL.

In most industries, enormous amounts of low-grade thermal energy are wasted. They are good potential for electricity generation. Teimouri and Behzadmehr [6] presented the performance of a 2D model of thermosyphonic MHDG numerically using Fortran code, at unsteady laminar natural convection flow. They used the liquid Gallium as the working fluid. Sawaya et al. [7] used a thermosyphon closed-loop MHD flow system to determine the Hall parameter of electrolyte solutions experimentally. Their working fluid was the NaCl and KCl solutions that have an electrical conductivity of 20 S/m. Liquid metal magnetohydrodynamic power generator (LM MHDG) can be used to utilize nuclear waste heat for electrical power generation. Satyamurthy et al. [8] presented the important and suitable parameters of LM MHDG when attached to the nuclear waste heat. They showed that the gross thermodynamic cycle efficiency varies from 4.9% to 20.1% over the cycle temperature range between 450 and 570 K. They proved the capability of LM MHDG in power generation using nuclear waste heat with good efficiency. The maximum electrical power density output in the vertical MHDG attached to a lead-cooled fast reactor with gravity as the driving force was analyzed by Ryan et al. [9]. The liquid metal Lead is the working fluid, which was chosen because it has a wide range of operating temperatures with appropriate thermal and electromagnetic properties. MHD molten salt pump found an application for nuclear reactor coolants and needs no moving mechanical parts as explained by Safi and Khater [10].

Solar heat can be used in LM MHDG as a heat source. Satyamurthy et al. [11] designed a two-phase LM MHDG system with solar and waste heat as a heat source for the generation of hydrogen. The system had two loops; Loop 1 had a liquid metal lead, Loop 2 had the liquid metal lead-bismuth as the electromagnetic working fluid, and the steam as the thermodynamic working fluid for both loops. They optimized important parameters like geometry, flow rate, etc. They could obtain 2.5 MW thermal power and 230 KW net electrical power with 9.2% net conversion efficiency.

Experimental and mathematical models of the MHD liquid sodium loop were studied by Saphier [12]. The simulation was developed to perform the dynamic analysis of the MHD loop using CSMP-III Simulation language. The experiment aimed to demonstrate the ability of MHD, DC generators to produce 20 kW of electricity. Also, the flow was regulated to stabilize the loop by a high-gain proportional controller, where it was stabilized at wide operating conditions.

MHDG can also be used to generate electrical energy in the sea and space, using the electromotive force of seawater crossing a magnetic field and thermoacoustic engine in space. This process is of low cost and high efficiency compared with the amount of electrical energy generated. Liu [13] compared the simulation results with the theoretical and experimental results of a 3D helical-type seawater MHDG system. They found a good agreement between the two. To progress the MHDG in the sea, the magnetic field and the efficiency of seawater flow in the generator must be enhanced. MHDG with thermoacoustic engine in space was investigated to convert mechanical energy, to an AC form of electrical energy theoretically and experimentally by Brekis et al.[14]. They concluded, that MHDG can be used as a primary source long distance Space mission.

The active and passive heat exchangers with MHD were studied by Alam and Kim [15]. They conclude that the MHD in passive heat exchangers enhanced the heat transfer rate and can be used to generate electrical power. The effects of chemical reaction on unsteady MHD flow past an impulsively started inclined plate with variable wall temperature and mass diffusion in the presence of Hall current were studied by Rajput and Kumar [16]. They applied a uniform magnetic field. The Governing equations were solved by the Laplace-transform technique. They concluded that the primary and secondary velocity increased with the increase in thermal Grashof number, mass Grashof Number, and time. The effect of thermal radiation and slip effects on the MHD boundary layer flow of tangent hyperbolic nanofluid were investigated by Shravani et al.[17]. Runge-Kutta fourth order method with the shooting technique was used. They concluded that the increase in velocity slip parameter leads to an increase in skin friction and Nusselt number.Singh and Kumar [18] illustrated the effects of a uniform magnetic field in micropolar fluid graphically on the fluid flow, couple stress coefficient and heat transfer characteristics.

Many studies were conducted to examine the effects of porosity under the influence of a magnetic field. The free convection on a vertical plate in porous media with variable wall temperature was studied by Singh and Kumar [19].They concluded that the magnetic field enhances the temperature, concentration, and wall couple stress. The lower stagnation point of a porous isothermal horizontal circular cylinder with MHD was studied by Uddin and Kumari [20,21]. Shareef [22] found primary and secondary fluid velocity reached to a different maximum value in the vicinity of the vertical plate and then decreased gradually.Kumar[23]studied the effects of the couple stress fluid flow on the magnetohydrodynamic with slip effect. Increasing the couple stress parameter leads to a decrease in the velocity distribution and an increase in the transverse velocity.

### *1.2. Single-Phase Natural Circulation loop (SPNCL)*

The single-phase natural circulation loop (SPNCL) is used due to failures that have occurred during the cooling process, especially in nuclear power plants. It works as a secondary cooling system when mechanical equipment fails. This is called a passive system. The circulation in SPNCL is caused by the temperature gradient that causes a density gradient. This drives the flow through the loop. The driving buoyancy force overcomes the loop frictional force. The SPNCL consists of heater, cooler and adiabatic piping sections as shown in **Figure 1.b**.

There are several experimental, numerical, and theoretical studies of SPNCLs [24-42]. There is a consensus between experimental studies, theoretical analyses, and numerical simulations about the steady-state, transient state, and stability of SPNCL. Different constant heat fluxes to the heater were considered. The SPNCL is used for different applications: as a cooling system in the nuclear reactor [24], for computer cooling [25], solar heating systems [26], gas turbine blade cooling [27],

geothermal power extraction [28], and other applications. Cheng et al. [29] solved the steady one-dimensional mathematical model SPNCL. Water was selected for working and secondary fluid. Constant heat flux was used as a boundary condition at the heater. It was observed that when the loop diameter increases the heat transfer rate, steady-state Reynolds number and Grashof number increase. However, the effect of loop diameter on the Grashof number was weak at a higher temperature difference.

Experimental and theoretical investigations of SPNCL at a steady state were reported by Cheng et al. [30], where the heating fluid temperatures were from 30 °C to 60 °C and the cooling fluid temperature was 10 °C, and a good agreement between theoretical and experimental results was observed. The steady and dynamic performance of the rectangular and toroidal natural circulation loops for heating and cooling with constant heat flux was studied by Basu et al. [31]. Meanwhile, the rectangular and toroidal models had been validated with experimental results, where the stable zone for the toroidal loop was wider than the rectangular loop at the same operating conditions.

Kumar and Gopal [32] presented a simple analytical expression of an SPNCL at steady-state with parallel flow heat exchangers using $CO_2$ as the secondary fluid in the loop and water as the external fluid in the heat exchangers. The temperature of $CO_2$ was found to affect the performance of the loop. Saha et al. [33] studied the thermohydraulic behavior of SPNCL at different power inputs numerically and experimentally at a steady state. They reported a good agreement between numerical and experimental results at low heater power input. Vijayan [34] tested the correlation of steady state Reynolds number of SPNCL for uniform and non-uniform diameter, with the experimental results. And tested the stability behavior of SPNCL by the relationship of the modified Stanton number and Grashof number. Their experimental results were found to match well with the correlation of steady state Reynolds number.

Minimizing the entropy generation is important to improve the performance of SPNCL. Goudarzi and Talebi [35] studied the effect of various loop dimensions and heater power on the circulation stability and entropy generation of SPNCL. Constant heat flux condition at the heater and constant wall temperature condition at the cooler was used in their calculations. Misale et al. [36] reported an experimental investigation about the effect of power transferred to the fluid and the inclination in SPNCL. Their study showed a stable behavior with a steady temperature difference across the heat sinks. The experimental and theoretical analyses of SPNCL were studied by Seyyedi et al. [37] who reported that the stability map had three regions: laminar, transient, and turbulent. Also, they found a good agreement about the effects of heater power input, inclination angle, and heat sink temperature between experimental and theoretical results.

Single-ended water-in-glass evacuated tubes with a diffuse reflector over them were used as a developer for the mass flow rate of single-phase natural circulation loops as presented by Budihardjo et al. [38]. Their experimental and numerical investigations showed the relationship between mass flow rate, solar input power, tank temperature, collector inclination, and tube aspect ratio. Hashemi-Tilehnoee et al. [39] studied the AKIAU-R-1P rectangular single-phase loop and found a good agreement between experimental results and the results of simulation of 1-D RELAP5/Mod3.2 code and 3-D ANSYS FLUENT computational fluid dynamic code. Mousavian et al. [40] used the finite difference method to solve the transient equations of SPNCL by RELAP5 code and used the Nyquist criterion to find the stability in SPNCL and reported a comparison with the experimental data. The 1-D and 3-D computational fluid dynamic codes of different configurations for a glass SPNCL were discussed by Pilkhwel et al. [41]. They presented the linear stability maps and transient flow behavior by CFD codes. Vijayan et al. [42] observed the instability oscillatory behavior of three different configurations of SPNCL using the computer code ATHLET.

### *1.3. Design of Experiments (DoE)*

Design of experiments (DOE) is one of the primary tools for applied statistics, that deals with analyzing the variability between factors. Factorial analysis and analysis of variance (ANOVA) tools are the most important tools for statistical analysis. The factorial analysis is used for identifying the most significant factors and interactions that affect the output response. Then, the response surface methodology (RSM) should be applied for the most significant interactions to optimize the output response.RSM is a collection of mathematical and statistical techniques that are useful for modeling and analysis in applications where a response of interest is influenced by several variables and the objective is to optimize this response [43]. The central composite design is a type of RSM, which is useful for building a second-order (quadratic) model for the response variable without needing to use a complete three-level factorial experiment. When the experimenter is relatively close to the optimum, a second-order model is usually required to approximate the response because of curvature in the true response surface and using a central composite design.

Reviewing the literature, it is found that the researchers presented analytical, numerical, and experimental results for MHDG at different working fluids. Steady-state and transient behavior of SPNCL were reported. The stability behavior of the system at different conditions was also investigated. However, to the authors' knowledge, no previous studies have been reported on the coupling between MHDG and SPNCL for systems with two pairs of magnets. The advantage of SPNCL LM MHDG is that there are no secondary vortices inside the loop, and it is a smooth generator in comparison with other generators. In the present work, the performance of a rectangular SPNCL coupled with two pairs of magnets, one on the heater and another one on the cooler for power generation will be numerically investigated, using the finite volume method. Moreover, the statistical analysis of SPNCL LM MHDG will be investigated, using factorial analysis and RSM by using statistical software. The proposed system will use low-temperature liquid metal to suit applications at low-grade energy.

## 2. Problem Statement

The basic system of SPNCL consists of a heater and cooler located on the right and the left legs of the loop, respectively. This study investigated the performance of rectangular SPNCL coupled with two pairs of magnets(SPNCL LM MHDG) using low-temperature liquid metal as the working fluid, one on the heater side and another one on the cooler side, as shown in **Figure 2**. The circulation in SPNCL is caused by the temperature gradient that causes a density gradient. This is what drives the flow through the loop. The driving buoyancy force overcomes the loop frictional resistance and provides the output MHDG power.

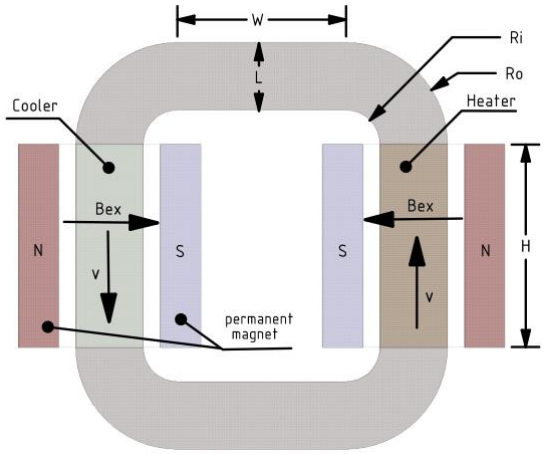


**Figure 2.** Schematic diagram of the rectangular SPNCL LM MHDG with two pairs of MHDGs.

An external magnetic field (Bex) is applied in the x-direction. The working fluid in MHDG is Mercury (Electrically Conductive Fluid). The performance of Mercury and Gallium is compared. **Table 1** shows the Properties of Mercury at Tref = 298.15 K.

The bottom pipe and top pipe are insulated. The heater, cooler, top pipe, and bottom pipe are electrically insulated. In this study, A laminar steady two-dimensional model of SPNCL LM MHDG is applied. The buoyancy driving force (the body force) is introduced into the momentum equation using the Boussinesq approximation. The Boussinesq approximation is used in this model for evaluating the density change as a function of the fluid temperature in the heater and cooler.

$$\rho = \rho_O\big(1 - \beta(T - T_O)\big) \quad (1)$$

The dimensions of the model are shown in **Figure 2**. The Height of the heater and cooler are equal to the Height of magnets and electrodes. The effects of Ra (heating effect), Ar (natural convection), and Ha (magnetic field strength) are numerically studied in this work. Where Ar is the Aspect ratio, and it is equal to H/L. For Ar = 3 the Height (H), length (L), width (W), inner radius (Ri) and outer radius (Ro) was 15, 5, 12.5, 2.5, and 7.5 mm respectively.

The parametric study is presented for 1E+03 < Ra < 1E+08, 3 < Ar < 24 and 10 < Ha < 1000. For simplicity, at Ar=3, the Ra must be between (1E+03 < Ra < 1E+06), because If Ra > 1E+06 then the flow will exceed the boiling point of Mercury and become unstable and Re assumes values greater than 2000 (Re > 2000), the limit for laminar flow. Where Re is an output parameter that indicates the average velocity of the working fluid.

## 3. Methodology

### *3.1. Mathematical Method*

For 2D incompressible laminar steady-state flow, subjected to body force represented by the Boussinesq term in the momentum equation, subjected to a magnetic field, and assuming electrically conductive fluid, the governing equations are as follows:

Continuity equation:

$$\frac{\partial U}{\partial X} + \frac{\partial V}{\partial X} = 0 \quad (2)$$

Define dimensionless parameters as follows,

$$X = \frac{x}{H}, Y = \frac{y}{H}, U = \frac{u}{v_o}, V = \frac{v}{v_o} \quad (3)$$

where, $v_o = \frac{\alpha}{H}$

In which $v_o$ is the referencevelocity and $\alpha$ is the thermal diffusivity which is equal:

$$\alpha = \frac{k}{\rho\, c_p} \quad (4)$$

Momentum equations can be written in the following form [3]:

$$U\frac{\partial U}{\partial X} + V\frac{\partial U}{\partial Y} = -\frac{\partial P}{\partial X} + Pr\left[\frac{\partial^2 U}{\partial X^2} + \frac{\partial^2 U}{\partial Y^2}\right] + Ra\,\mathrm{Pr}\;\theta \quad (5)$$

$$U\frac{\partial V}{\partial X} + V\frac{\partial V}{\partial Y} = -\frac{\partial P}{\partial Y} + Pr\left[\frac{\partial^2 V}{\partial X^2} + \frac{\partial^2 V}{\partial Y^2}\right] - Ha^2\,\mathrm{Pr}\,V \quad (6)$$

where, P, Pr, Ra, and *Ha are* the dimensionless pressure, Prandtl number, Rayleigh number, and Hartmann number respectively, which are defined as follows:

$$P = \frac{p}{p_o} \text{ where, } p_o = \rho\, {v_o}^2 \quad (7)$$

$$Pr = \frac{\mu}{\rho\, c_p}, Ra = \frac{g\,\beta\,\Delta T\, H^3}{\alpha\, v} \text{ where, } v = \frac{\mu}{\rho} \quad (8)$$

$$Ha = \frac{B_{ex}}{B_o} \text{ where, } B_o = \frac{1}{H\sqrt{\frac{\sigma}{\mu}}} \quad (9)$$

where,$p_o$, $g, \beta, v$, $B_o$ and $\sigma$are the reference pressure, gravitational acceleration, coefficient of thermal expansion, kinematic viscosity, reference magnetic field, and electrical conductivity of liquid metal, respectively.

**Table 1.** The Properties of Mercury and Gallium at Tref = 298.15 and 349 K respectively.

| TLM | μ (Kg/m.s) | ρ ($Kg/m^3$) | $C_p$ (J/Kg. K) | β (1/K) | k (W/m.K) | σ (siemens/m) | Pr | Melting point (°C) | Boiling point (°C) |
|---|---|---|---|---|---|---|---|---|---|
| Mercury | 1.523E-03 | 13529 | 139.3 | 1.8E-04 | 8.54 | 1.044E06 | 0.025 | 38.83 | 356.73 |
| Gallium | 1.73E-03 | 6060 | 386.1 | 1.27E-04 | 33.39 | 3.74E06 | 0.02 | 29.76 | 2204 |

Energy equation [3]:

$$U\frac{\partial\theta}{\partial X}+V\frac{\partial\theta}{\partial Y}=\left[\frac{\partial^2\theta}{\partial X^2}+\frac{\partial^2\theta}{\partial Y^2}\right]+Ec_mHa^2\,\mathrm{Pr}\,V^2 \quad (10)$$

where, $\theta, Ec$ and $Ec_m$are the dimensionless temperature, Eckert number, and modified Eckert number respectively, which are defined as follows:

$$\theta=\frac{T-T_o}{\Delta T}\text{ where, }\Delta T=T_h-T_c\text{ and }T_o=\frac{T_h+T_c}{2} \quad (11)$$

$$Ec=\frac{{v_o}^2}{c_p\,\Delta T},Ec_m=\frac{\alpha^2}{H^2\,c_p\,\Delta T} \quad (12)$$

In which$T_h$,$T_c$, $\Delta T$ and $T_o$ are the temperature of the heater, the temperature of the cooler, the Temperature difference, and the mean temperature, respectively.

The Reynolds number and Nusselt number are defined as below:

$$Re=\frac{\rho\,v_{Avg}\,L}{\mu},Nu=\frac{h\,L}{K} \quad (13)$$

Where, $v_{avg}$ is the average velocity and $h$ is the heat transfer coefficient. Also, the Reynolds number is defined based on the hydraulic diameter,$D_h=L$.

The dimensionless current density J* which is equal [3]:

$$J^*=\frac{J}{J_o}\text{ where, }J_o=\sigma\,v_oB_o=\frac{\sigma\,\alpha\,B_o}{H},J=-\frac{\alpha\sqrt{\sigma\,\mu}}{H^2}\,V\,Ha \quad (14)$$

Where, $J_o$is the current density reference.

The dimensionless generated electrical powerW* which is equal [3]:

$$W^*=\frac{w}{w_o}\text{ where, }w_o=\sigma\,{v_o}^2{B_o}^2,w=-J\,v_{Avg}B \quad (15)$$

Where, $w_o$, $B_o$ and $v_o$ are the electrical power reference, the magnetic field reference, and the velocity reference which is $v_o=\alpha/H$, respectively.

### *3.2. Numerical Method*

The governing equations of SPNCL LM MHDG including, continuity, momentum, energy, and hydrodynamic equations have been solved using numerical software. A 2D planar geometry of MHDG has been drawn to make a parametric study at different Ar.

The quality of the mesh plays a significant role in the accuracy and stability of the numerical computation. A uniform all-triangle meshes type is applied with inflation layers near the walls. The attributes associated with mesh quality are node point distribution, smoothness, and skewness. For the same cell count, triangular meshes will give more accurate solutions than quadrilateral meshes. The aspect ratio of uniform mesh (ideal) is almost equal to 1 and the change in size should be gradual (smooth). The mesh density should be high enough near the walls (fine) to capture all relevant flow features such as to resolve the boundary layer flow, by using inflation layers.

The coupled pressure-based solver has been used, where the governing equations are solved using the finite volume method. The coupled algorithm solves the momentum and pressure-based continuity equations together. The full implicit coupling is achieved through an implicit discretization of pressure gradient terms in the momentum equations and an implicit discretization of the face mass flux. The momentum, Energy, and the external magnetic field in the x and y direction are discretized using a second-order central difference scheme. The second-order central difference scheme provides improvement over the standard and linear schemes. The body-force-weighted scheme is selected for the pressure, by assuming that the normal gradient of the difference between pressure and body forces is constant. This works well for buoyancy calculations.The solution is assumed to vary linearly, by using Least Squares Cell-Based Gradient. The gravitational acceleration in the y-direction is employed. The Boussinesq approximation is used in the density of the liquid metal. The buoyancy driving force (the body force) is introduced into the momentum equation using the Boussinesq approximation. The Boussinesq approximation is used in this model for evaluating the density change as a function of the fluid temperature in the heater and cooler.

MHD equation is solved under relaxation factor 0.9, where DC filed type, Lorentz force, and joule heating have been included. Two magnetic field regions are identified for the heater and cooler. Operating conditions have been changed, where the operating pressure and operating temperature of Mercury and Gallium are 101325 pascals, 298.15 K, and 101325 pascals, 349 K, respectively. Reference values computed from the heater are based on the properties of the type of liquid metal and the dimensions of the model. For evaluating force or moment coefficients, Reynolds number, or some other derived quantities, it must be set reference values which depend upon the geometry and flow conditions. Otherwise, end up getting unrealistic values of coefficients even though the solution is converged. The model is very complicated with natural convection and magnetic field. The solution converged when the absolute residual criteria for continuity, momentum, energy, and magnetic field were 1E-04, 1E-06, 1E-06, and 1E-05, respectively. Hybrid initial guess uses the boundary conditions and then solves Euler problems. It uses the solution to this Euler problem as the initial guess. standard initial guess needs to provide the initial guess. The hybrid initial guess is more beneficial in multi-input parameters such as natural convection and magnetic field.

### *3.3. Statistical Method*

The statistical analysis of SPNCL LM MHDG is investigated, using factorial analysis and response surface method by using statistical software. Where the Statistical analysis is presented for Ra, Ar, Ha, and TLM. Where the Factorial analysis is presented for 1E+03 < Ra < 1E+06, 3 < Ar < 24, 10 < Ha < 1000, and TLM (Mercury and Gallium).

The Ra was chosen between 1E+03 and 1E+06 because, at Ar = 3, the Ra must be between (1E+03 < Ra < 1E+06). If Ra > 1E+06 at Ar = 3 then the flow will exceed the boiling point of Mercury and become unstable, Re > 2000, exceeds the laminar flow limit. Then 1E+03 < Ra < 1E+06 is the best choice for all Aspect ratios.**Table 2** shows the limitations of the Ra at different Ar for Mercury.

**Table 2.** The limitations of the Rayleigh number (Ra) at different Aspect ratios (Ar) for Mercury.

| Ar | 3 | 6 | 12 | 24 |
|---|---|---|---|---|
| Ra | 1E+03 to 1E+06 | 1E+03 to 1E+07 | 1E+03 to 1E+07 | 1E+03 to 1E+08 |
| Re | Less than 2000 | Less than 2000 | Less than 2000 | Less than 2000 |

A factorial analysis is used for identifying the most significant factors and interactions that affect the generated electrical current. The response surface methodology is applied for the most significant interactions to optimize the

response of the generated electrical power, using a central composite design.

## 4. Validation

The performance of the 2D model of thermosyphonic MHDG numerically as shown in **Figure 3**, using finite volume technique for laminar natural convection flow was analyzed using Fortran code by Teimouri and Behzadmehr [6][3]. L=width, H=height and He denote the height of electrodes and are equal to the height of the baffle. The distance between the baffle and the top wall and the bottom wall is equal to L/2. The thickness of the baffle is negligible. Ar is the ratio of height to width of the thermosyphon, H/L. An isothermal heat source with the temperature Th, and a heat sink with a constant temperature of Tc, Th > Tc are considered along with the left and the right sidewalls, respectively. The bottom wall, top wall, and baffle are insulated. The left, right, top, and bottom walls are electrically insulated. The Magnetic field of strength B is applied horizontally parallel to the x-axis. They used the liquid Gallium as the working fluid. The properties of liquid Gallium at 349 K are shown in Table 1. They investigated the effects of Ra, Ha, Ar, and electrical efficiency (K) on the generated power (W). They found that by increasing the Rayleigh number the generated power (W), electric current density (J), and electric field (E) increase.

The 2D thermosyphonic MHDG problem with liquid Gallium working fluid solved by Teimouri and Behzadmehr [3] using Fortran code was verified against a numerical software solution. Discrepancies between the two results were less than 5%. The present problem numerical software solution is validated against the Teimouri and Behzadmehr program. Results are found to agree within 5% too. A 2D planar geometry of the Thermosyphonic model has been drawn to make a parametric study at different Aspect ratios, in which Ar is equal to H/L.

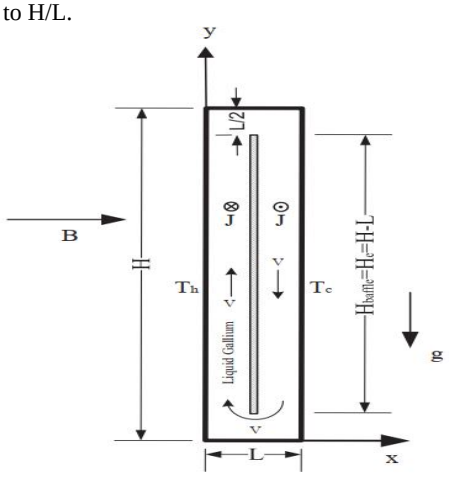


**Figure 3.** Simplified geometry of the thermosyphon in the presence of a magnetic field [3].

A uniform all-triangle meshes type is applied with inflation layers near the walls and all assumption has been mentioned in the numerical method section. But the operating pressure and operating temperature of liquid Gallium are 101325 pascals and 349 K respectively. The comparison between Fortran code and the 2D model of CFD code (numerical software) results is presented a good agreement between them. Where **Table 3** presents the maximum generated J* for the best Ar and Ha at 1E+03 < Ra < 1E+07 with a deviation of less than 5%. And that showed J* is the maximum increase with Ra. In which the J* is the dimensionless current density as shown in Eq.14.

**Table 3.** Generated J* at Gallium for the best Ar and Ha among the considered ranges for different Rayleigh numbers.

| Ra | Best Ar | Best Ha | J* (Ref. 3 results) | J* (present results) | deviation |
|---|---|---|---|---|---|
| 1E+03 | 2 | 10 | 9.38E0 | 9.106E0 | 2.95% |
| 1E+04 | 2 | 50 | 6.12E1 | 5.914E1 | 3.37% |
| 1E+05 | 5 | 50 | 4.93E2 | 5.127E2 | 4.01% |
| 1E+06 | 5 | 100 | 2.98E3 | 3.077E3 | 3.26% |
| 1E+07 | 10 | 500 | 8.83E3 | 9.243E3 | 4.68% |

## 5. Mesh quality check

The mesh type of SPNCL LM MHDG that has been applied is a uniform all-triangle mesh type with inflation layers near the walls. **Figure 4** shows the triangle mesh with inflation layers of the heater at Ar = 3, where inflation layers are equal to 10 with 1 growth rate.

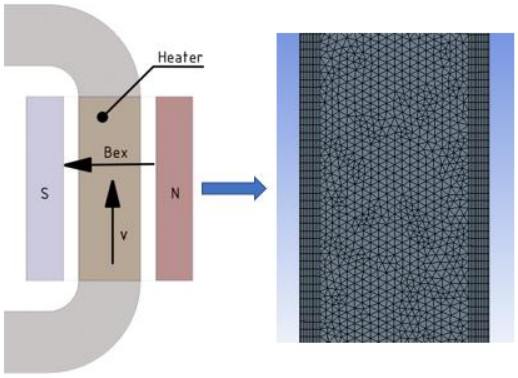


**Figure 4.** The mesh type of heater in SPNCL LM MHDG at Ar = 3.

Improving the mesh quality before proceeding with simulation is important and plays a significant role in the accuracy and stability of the numerical computation. Also, it detects any mesh trouble before getting started with the problem setup. **Table 4** shows the dimensionless generated electrical power from the heater and cooler (two pairs of magnets), average Nusselt number ($Nu_{avg}$) and Reynolds number (Re) at Element size between 0.5 to 0.1 mm for Ar = 3, Ra = 1E+06, and Ha = 100. In which the W* is the dimensionless generated electrical power as shown in Eq.15.

**Table 4.** Mesh quality check for Ar = 3, Ra = 1E+06, and Ha = 100 at Element size between 0.5 to 0.1 mm for Mercury.

| Case | Element size (mm) | # of Nodes | # of Elements | W* | $Nu_{avg}$ | Re |
|---|---|---|---|---|---|---|
| **1** | 0.5 | 4536 | 5244 | 5.79E+07 | 13.4493 | 730.515 |
| **2** | 0.4 | 6259 | 7722 | 6.38E+07 | 13.5858 | 774.837 |
| **3** | 0.3 | 9633 | 12930 | 6.96E+07 | 13.6343 | 806.234 |
| **4** | 0.2 | 18160 | 26772 | 8.35E+07 | 13.7215 | 876.813 |
| **5** | 0.15 | 29848 | 47024 | 8.39E+07 | 13.7229 | 877.826 |
| **6** | 0.1 | 58373 | 97738 | 8.42E+07 | 13.7232 | 879.539 |

 

As Table 4 shows case number 4 at Element size = 0.2 will be adopted, which is sufficiently fine, stable, and economical to ensure the accuracy and stability of the numerical computation. Cases with less element size (< 0.2 mm) are barely stable. The accuracy and stability for dimensionless vertical velocity profile in heater for Ar = 3, Ra = 1E+06, and Ha = 100 at different Element sizes are shown in **Figure 5**. Again, mesh with element size = 0.2, proved to be the most appropriate for accuracy and stability.

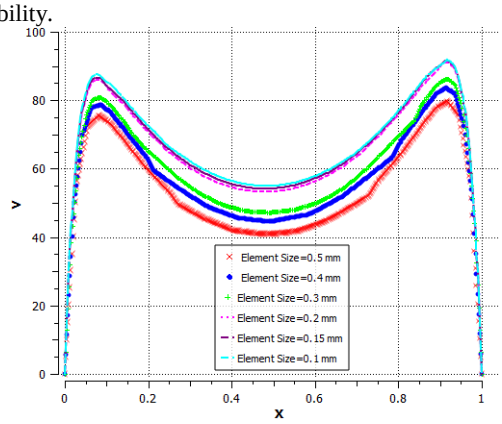


**Figure 5.** Dimensionless vertical velocity profile in the heater at Ar = 3, Ra = 1E+06, and Ha = 100 at different Element sizes for Mercury.

## 6. Results

### *6.1. CFD results*

In the present work, the governing equations of SPNCL LM MHDG have been numerically investigated, using the finite volume method by using numerical software. A 2D model of SPNCL LM MHDG with two pairs of magnetsis drawn as mentioned in the numerical method section. The parametric study is presented for 1E+03 < Ra < 1E+08, 3 < Ar < 24 and 10 < Ha < 1000 for Mercury as the working fluid. Moreover, the performance of Mercury and Gallium is compared as shown in **Figure 11.** The comparison between SPNCL and Thermosyphon MHDG is presented in **Table 5**.

#### *6.1.1. The stability (Stream Function and Isotherms)*

The advantage of SPNCL is that there are no secondary vortices inside the loop in comparison with the geometry used by Ref. 3. This obvious in

**Figure 6**, which shows the stream function contours. The flow is oscillatory at Ha = 10 and Ha = 50 and becomes stable at Ha = 100 and becomes more stable with increasing Ha.

Lorentz force reduces the buoyancy force, and increasing Ha decreases the natural convection. Cases with Ra = 1E+04 are more stable than those with Ra = 1E+05 at Ha = 100. Larger Ra means larger $\Delta T$ and thus higher natural convection effect and lower magnetic field effect (the Lorentz Force). Also, the stability and oscillatory have appeared in Isotherm contours as shown in **Figure 7**.

Furthermore, decreasing the Ra leads to a decrease in the maximum velocity at the same Ha and Ar in the SPNCL LM MHDG, and it becomes very low and tends to zero as shown in **Figure 8.a**, where it presents the velocity profile at the heater section in SPNCl LM MHDG for different Ra at Ar = 3 and Ha = 100.

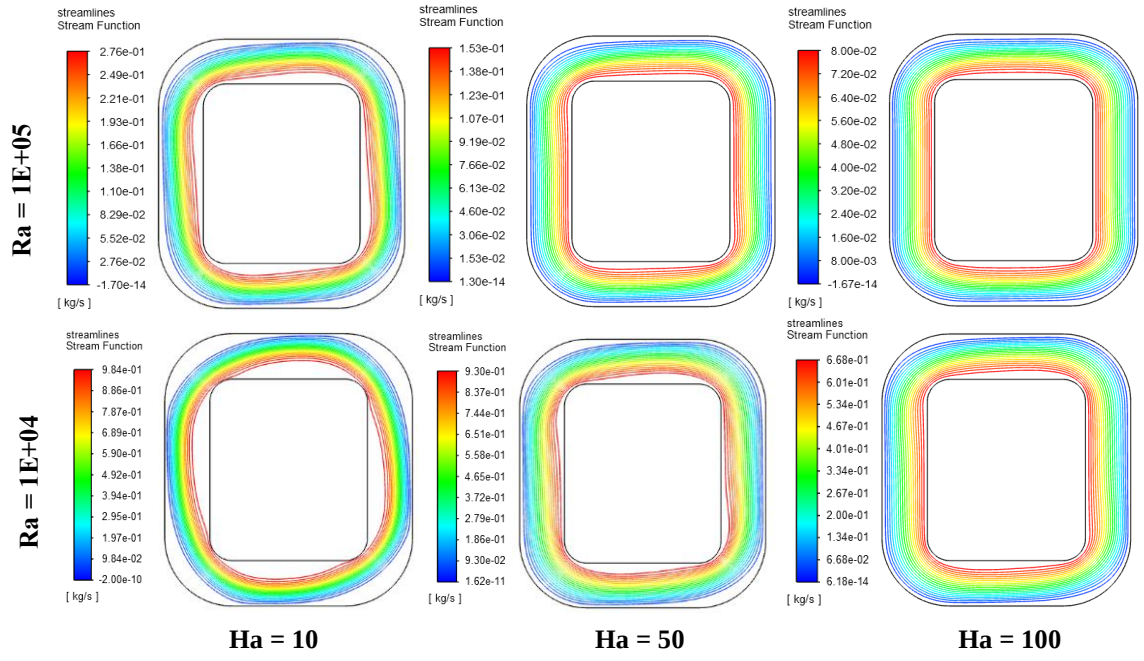


**Figure 6.** The stream function contours of SPNCL LM MHDG for Ar = 3 at different Ra and Ha for Mercury.

*6.1.2. The velocity profile at the heater section*

Furthermore, increasing the Ha leads to a decrease in the maximum velocity in the SPNCL LM MHDG, and it becomes extremely low and tends to zero as shown in **Figure 8.b**, where it presents the dimensionless vertical velocity profile at the heater section in SPNCl LM MHDG for different Ha at Ar = 3 and Ra = 1E+06. In this case, the flow is oscillatory and becomes more stable with increasing Ha. For simplicity, the Ha should be greater than 100 to get stability. The velocity profile at the cooler section also shows the same kind of trend as the velocity profile at the heater section.

Dimensionless Vertical velocity profile, at the middle height of the heater for various Ha numbers at Ar = 6 and 12, and Ra = 1E+04 is presented in **Fig. S1 (in the appendix)**. Increasing the aspect ratio reduces the oscillatory and the velocity profile becomes fully developed, more symmetric, and stable.

*6.1.3. Reynolds Number*

On the other hand, the Re increases with the increase of the Ra and decreases with increasing the Ha as shown in **Figure 9.a**, where it presents the relationship between Re and Ha for different Ra at Ar = 12.

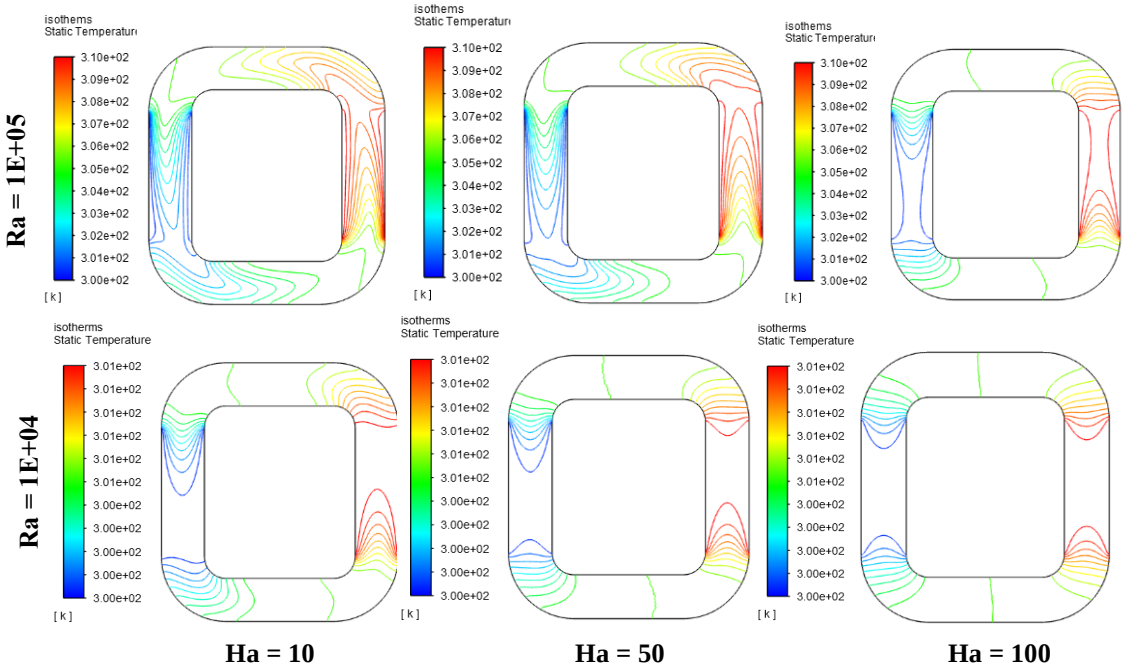


**Figure 7.** The isotherms contours of SPNCL LM MHDG for Ar = 3 at different Ra and Ha for Mercury.

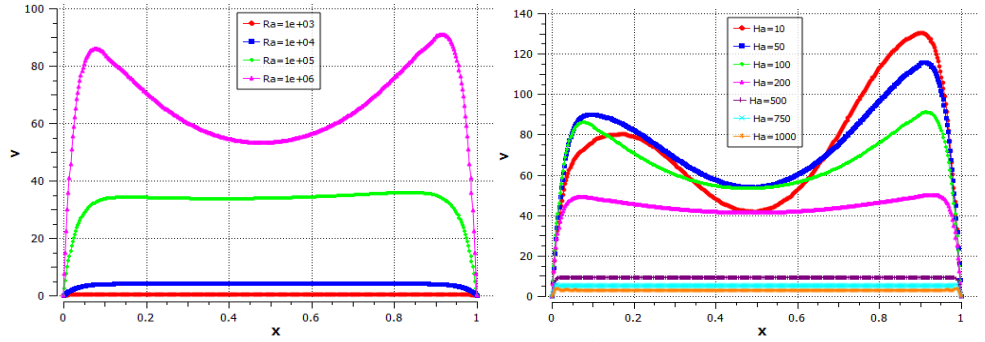


**a.)** Different Ra (Ha =100) b.) Different Ha (Ra = 1E+06)

**Figure 8.** The dimensionless vertical velocity profile at the heater section in SPNCl LM MHDG at Ar = 3 for Mercury.

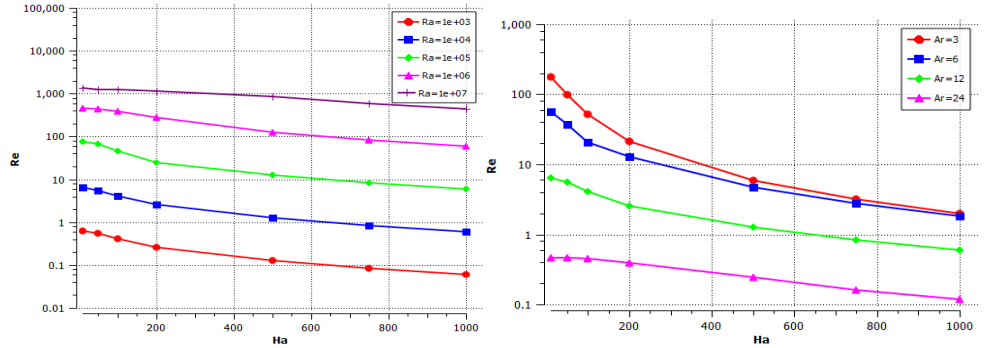


a.) Different Ra (Ar =12) b.) Different Ar ( Ra = 1E+04)

**Figure 9.** The relationship between Re and Ha for Mercury.

 

Increasing the Ha and Ar it is possible to have stable results in higher Ra. Because that leads to a decrease $\Delta T$ in the higher Ar. **Figure 9.b** presents the relationship between Re and Ha for different Ar at Ra = 1E+04. Where the Re decreases with the increase of the Ar and the Ha.

*6.1.4. Average Nusselt Number*

The Nu increases with the increase of the Ar and the Ra. **Figure 10** presents the relationship between $Nu_{Avg}$ of heater walls **(hot walls)** and Ra for different Ar at Ha = 100. Where, the increase in the Ar leads to an increase in the required Ra, which is effective on the average Nusselt number. For instance, At Ar = 6, 12, and 24 the effect of natural convection began to appear at Ra > 1E+05, Ra > 1E+06, and Ra > 1E+07 respectively. Therefore, increasing the Ar requires an increase in Ra to continue the fluid circulation within the loop effectively, that is, to maintain the effect of natural convection. Where the Nu is calculated by finding the heat transfer coefficient $(h)$ of heater walls **(hot walls)** as shown in Eq.13.

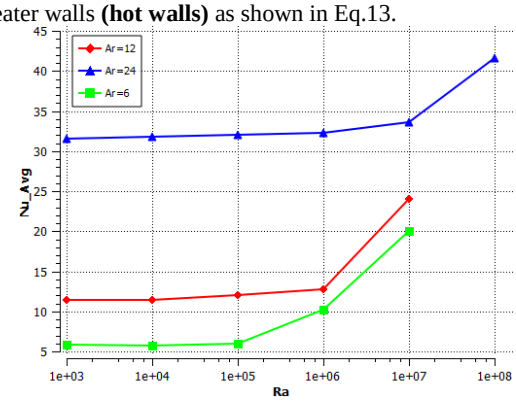


**Figure 10.** The relationship between $Nu_{Avg}$ of heater walls and Ra for Mercury at different Ar (Ha =100).

*6.1.5. Generated Electrical Current and Power*

The SPNCL LM MHDG is characterized as a smooth generator in comparison with the thermosyphon MHDG. Thermosyphon MHDG contains corners, this creates secondary vortices that have a negative effect on the performance of the generator. **Table 5** shows the dimensionless generated electrical current (J*) of Thermosyphon and SPNCL MHDGs for liquid gallium as the working fluid. where, the electrical current generated by the SPNCL LM MHDG is better than the thermosyphon MHDG, by about 13%.

**Table 5.** Dimensionless generated electrical current (J*) of Thermosyphon and SPNCL MHDGs for liquid gallium.

| Ar | Ra | Ha | J*(Thermosyphon) | J*(SPNCL) | %increase |
|---|---|---|---|---|---|
| 3 | 1.00E+04 | 10 | 2.18E+03 | 2.41E+03 | 10.44% |
| 3 | 1.00E+04 | 50 | 3.19E+03 | 3.57E+03 | 12.03% |
| 3 | 1.00E+04 | 100 | 3.13E+03 | 3.55E+03 | 13.33% |
| 3 | 1.00E+04 | 200 | 2.21E+03 | 2.46E+03 | 11.4% |
| 3 | 1.00E+04 | 500 | 9.80E+02 | 1.10E+03 | 12.05% |
| 3 | 1.00E+04 | 750 | 6.47E+02 | 7.12E+02 | 10.04% |
| 3 | 1.00E+04 | 1000 | 5.13E+02 | 5.60E+02 | 9.29% |

As it was mentioned, Increasing the Ra leads to an increase in the Re, and the natural convection becomes more effective. Also, the Re decreases with the increase of the Ar and the Ha. In this study, there is a best Ar and Ha to obtain the maximum electrical power at different Ra as shown in Table 6.

The best Ar and generated electrical power increase with the increase in Ra as shown in Table 6. But each case needs a certain Ha to obtain the maximum electrical power. Where the generated electrical power and current for the heater and cooler (two pairs of magnets). Moreover, by comparing the performance of mercury with Gallium, gallium generates more electrical power than mercury. Because the electrical conductivity of gallium is higher than that of mercury.

The results show that there is the best Ha (maximum Ha) for each Ra to obtain the maximum electrical power as shown in **Figure 11.a.** where increasing the Ra increases the Re, and then generated power increases. For instance, the maximum Ha to generate the maximum electrical power at Ar = 3 and Ra = 1E+03, 1E+04, 1E+05, and 1E+06, was 100, 100, 100, and 200 respectively.

**Table 6.** Generated electrical power for the best Ar and Ha for different Rayleigh numbers with two pairs of magnets (Mercury and Gallium are the working fluid).

| Ra | Best Ar | Best Ha | W(Mercury) mW | W*(Mercury) | Ar | Ha | W(Gallium) mW | W*(Gallium) |
|---|---|---|---|---|---|---|---|---|
| 1.00E+03 | 3 | 100 | 3.87E-03 | 2.55E+03 | 3 | 100 | 9.17E-03 | 2.24E+04 |
| 1.00E+04 | 3 | 100 | 4.04E-02 | 2.56E+05 | 3 | 100 | 7.14E-02 | 2.18E+06 |
| 1.00E+05 | 3 | 100 | 3.25E-01 | 1.86E+07 | 3 | 100 | 9.82E-01 | 1.58E+08 |
| 1.00E+06 | 6 | 200 | 1.26E+00 | 1.06E+09 | 6 | 200 | 5.46E+00 | 5.49E+09 |
| 1.00E+07 | 12 | 500 | 3.27E+00 | 2.95E+10 | 12 | 500 | 1.94E+01 | 2.91E+11 |
| 1.00E+08 | 24 | 1000 | 8.46E+00 | 7.85E+11 | 24 | 1000 | 4.75E+01 | 6.95E+12 |

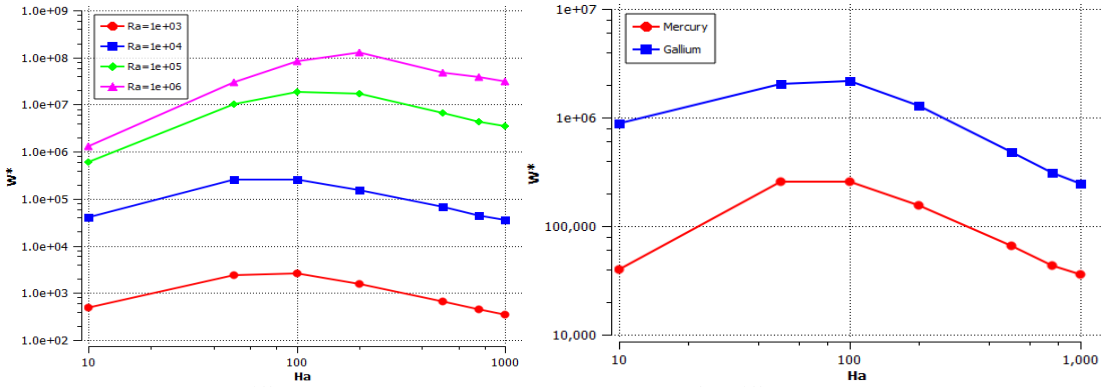


a.) Different Ra (Mercury) b.) Different TLM (Ra = 1E+4)

**Figure 11.** The relationship between Ha and W* at Ar = 3.

For clarity, the results show that gallium generates more electrical power than mercury in **Figure 11.b**. Furthermore, there is the best Ha (maximum Ha) for each working fluid to obtain the maximum electrical power. Because the velocity of the working fluid becomes extremely low and tends to zero after reaching maximum Ha.

The value of Ha and generated electrical power depends on the aspect ratio and Ra. **Table 8** shows the Dimensionless generated electrical power and current (two pairs of magnets) for the best Ra and Ha at different Ar. Increasing the Ar requires an increase in the Ra and Ha to obtain the maximum electrical power. Gallium generates more electrical power than mercury.

### *6.2. Statistical analysis results*

#### *6.2.1. Factorial analysis*

The parametric study of a 2D model of SPNCL LM MHDG with two pairs of magnetsresults is presented previously. Based on the parametric study of the generated electrical power, Statistical analysis of SPNCL LM MHDG is studied, using statistical software in this section. The effect of Ra, Ar, Ha, and TLM on the generated electrical power is studied by using factorial analysis and response surface method. Where the Statistical analysis is presented for low, medium, and high values of Ra, Ar, Ha, and TLM for $3^3$ factorial design, as shown in **Table 7**.

**Table 7.** Low, medium, and high values for factors.

| Factor | Type of factor | Level | | |
|---|---|---|---|---|
| | | Low | Medium | High |
| TLM | Categorical factor | Mercury | - | Gallium |
| Ar | Continuous factor | 3 | 6 | 24 |
| Ra | Continuous factor | 1E+03 | 1E+04 | 1E+06 |
| Ha | Continuous factor | 10 | 500 | 1000 |

The Ra was chosen between 1E+03 and 1E+06 because, at Ar = 3, the Ra must be between 1E+03 < Ra < 1E+06. If Ra > 1E+06 at Ar = 3 then the flow will exceed the boiling point of Mercury and become unstable and Re > 2000. Then 1E+03 < Ra < 1E+06 is the best choice for all Aspect ratios as shown in Table 2. The factors that are identified as significant are investigated using factorial analysis. Ra, Ha, and Ar in the statistical mathematical model of SPNCL LM MHDG are significant as shown in **Fig. 12**. But Rayleigh number (Ra) is the most significant factor (Dominant Factor).

The Pareto chart of the effects clearly shows that Ra is dominant, followed by Ha, and Ar. The significant factors and interactions are summarized in **Fig. S2 (in the appendix)** for Mercury and Gallium. For clarity, **Fig. S3.a** and **Fig. S3.b (in the appendix)** present the main and interaction effects plots for generated electrical power.

Moreover, a normal probability plot of the residuals for dimensionless generated electrical power as a response is shown in **Fig. S4 (in the appendix)**. The residuals are fairly linear along a straight line, which indicates there are no suspicions of any problem with normality in the data. furthermore, there are no indications of severe outliers.

#### *6.2.2. Response Surface Methodology*

Response surface methodology (RSM) is a collection of mathematical and statistical techniques that are useful for modeling and analysis in applications where a response of interest is influenced by several variables and the objective is to optimize this response. The response surface methodology is applied for the most significant interactions to optimize the response of the generated electrical power, using a central composite design. The RSM is applied at Ra, Ha, and Ar for generated electrical power (Mercury and Gallium) as the response, where the regression equations for Mercury and Gallium are as follows:

- Mercury:

$$W(mW) = -0.364 + 0.000001\,Ar + 0.0855\,Ra + 0.000518\,Ha + 0.00299\,Ra*Ra - 0.000004\,Ar*Ha + 0.000001\,Ar*Ra \quad (16)$$

- Gallium:

$$W(mW) = -1.972 + 0.000020\,Ar + 0.529\,Ra + 0.00153\,Ha + 0.01916\,Ra * Ra - 0.000002\,Ha * Ha + 0.000005\,Ar * Ha \quad (17)$$

The maximum generated electrical power can be obtained in the green zone as shown in **Figure 13**, where the contour plot of generated electrical power shows that the Ha and Ra should be 1000 and 1E+06, respectively at the average Ar to obtain the maximum electrical power for Mercury, and Ra should be 500 and 5E+05, respectively at the average Ar to obtain the maximum electrical power for Gallium. It is important to note that an increase in Ha requires an increase in Ra to continue the fluid circulation within the loop effectively, that is, to maintain the effect of natural convection, as was mentioned in CFD Results.

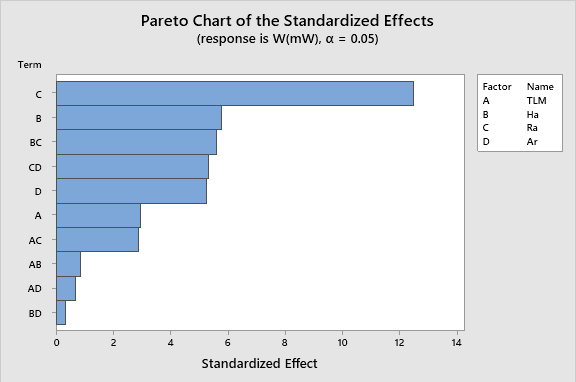


**Fig. 12:** Pareto chart of the standardized effects for (Rayleigh number (Ra), Hartmann number (Ha), and Type of Liquid Metal (TLM)) for generated electrical power.

**Table 8.** Generated electrical power for the best Ra and Ha at different Ar with two pairs of magnets (Mercury and Gallium are the working fluid).

| Ar | Best Ra | Best Ha | W(Mercury) mW | W* (Mercury) | Ra | Ha | W(Gallium)mW | W* (Gallium) |
|---|---|---|---|---|---|---|---|---|
| 3 | 1.00E+06 | 200 | 7.73E-01 | 1.28E+08 | 1.00E+06 | 200 | 8.64E-01 | 2.70E+09 |
| 6 | 1.00E+07 | 750 | 5.68E+00 | 3.20E+10 | 1.00E+07 | 750 | 9.17E+00 | 2.95E+11 |
| 12 | 1.00E+07 | 500 | 3.27E+00 | 2.95E+10 | 1.00E+07 | 500 | 1.94E+01 | 2.91E+11 |
| 24 | 1.00E+08 | 1000 | 8.46E+00 | 7.85E+11 | 1.00E+08 | 1000 | 4.75E+01 | 6.95E+12 |

 

Moreover, the maximum generated electrical power can be obtained in the green zone as shown in **Fig. S5 (in the appendix)**. Where the contour plot of generated electrical power shows that the Ar and Ra should be 12.5 and 1E+06, respectively at the average Ha to obtain the maximum electrical power for Mercury, 12.5 and 5.5E+05, respectively obtain the maximum electrical power for Gallium.

*6.2.3. Optimal Design Condition*

Optimal conditions are found using RSM as a Response Optimizer, to identify the combination of input variable settings that optimize the generated electrical power and evaluate the impact of multiple variables on a response. The Maximum generated power at factors (Ra, Ha, and Ar) for Mercury and Gallium is presented in**Table 9**

**Table 10.** The Maximum generated power in RSM.

| TLM | Ra | Ha | Ar | Max. Power (mW) |
|---|---|---|---|---|
| Mercury | 818364 | 700 | 11.9091 | 0.656384 |
| Gallium | 525727 | 510 | 13.1818 | 7.162650 |

For clarity, according to the RSM Results, **Fig. S6 (in the appendix)** shows that the maximum power for Mercury is 0.656384 mW at Ar = 11.9091, Ra = 818364, and Ha = 700, and the maximum power for Gallium is 7.162650 mW at Ar = 13.1818, Ra = 525727 and Ha = 510.

## 7. Conclusion

The parametric study of SPNCL LM MHDG has been numerically investigated, using the finite volume method, using numerical software. Using low-temperature liquid metal as the working fluid with two pairs of magnets, one on the heater side and another one on the cooler side, where two magnetic field regions are identified for the heater and cooler. The parametric study is presented for Ra, Ar, and Ha numbers for Mercury and Gallium as the working fluid. Moreover, the statistical analysis of SPNCL LM MHDG has been investigated, using factorial analysis and response surface method by using statistical software. Based on the numerical and statistical investigations, the following conclusions can be made:

1. Lorentz force reduces the buoyancy force, where increasing Ha decreases the natural convection effect and the secondary vortices that have a negative effect on the performance of the generator. The advantage point of SPNCL is that there are no secondary vortices inside the loop like the thermosyphon loop.
2. Decreasing the Ra and increasing the Ha decreases the maximum velocity, and it becomes very low and tends to zero.
3. Increasing the Ar reduces the oscillatory and the velocity profile becomes fully developed, more symmetric, and stable.
4. Increasing the Ra increases the Re, and increasing Ha and Ar decreases Re.
5. Increasing the Ra and Ar increases the Nu. Therefore, increasing the Ar requires an increase in Ra to continue the fluid circulation within the loop effectively, that is, to maintain the effect of natural convection.
6. Increasing the Ar requires an increase in the Ra and Ha to obtain the maximum electrical power.
7. Increasing the Ra increases the Re, and then generated power increases.
8. The electrical current generated by the SPNCL LM MHDG is better than the thermosyphon MHDG, by about 13%.
9. Ra is the most significant factor in the statistical analysis. In optimal conditions, the maximum power for Mercury is 0.656384 mW at Ar = 11.9091, Ra = 818364, and Ha = 700, and the maximum power for Gallium is 7.162650 mW at Ar = 13.1818, Ra = 525727 and Ha = 510.
10. The statistical results using the response surface method presented a fair agreement with the existing CFD results.

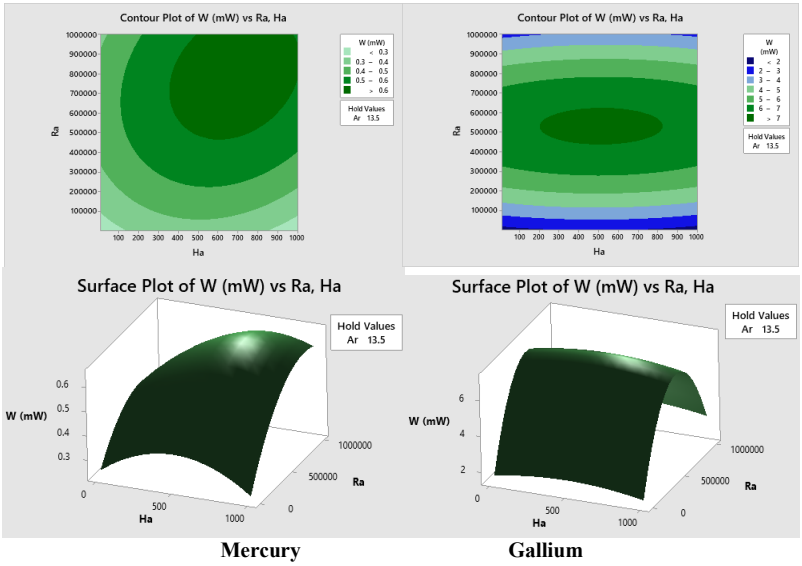


**Mercury** **Gallium**

**Figure 13.** Contour and surface plot of generated electrical power vs Rayleigh number (Ra),Hartmann number (Ha) for Mercury and Gallium.

## References


[1] S. C. Kaushik, S. S. Verma, A. Chandra, "Solar-assisted liquid metal MHD power generation: a state of the art study", Heat Recovery Systems & CHP, Vol. 15, No. 7, 1995, pp. 675-689. https://doi.org/10.1016/0890-4332(95)90047-0.

[2] E. Cosoroaba et al., "3D multiphysics simulation and analysis of a low temperature liquid metal magnetohydrodynamic power generator prototype", Sustainable Energy Technologies and Assessments, vol. 35, 2019, pp. 180–188. https://doi.org/10.1016/j.seta.2019.05.012.

[3] X. D. Niu, H. Yamaguchi, X. J. Ye, Y. Iwamoto, "Characteristics of a MHD power generator using a low-melting-point Gallium alloy", Electrical Engineering, vol. 96, no. 1, 2014, pp. 37–43. https://doi.org/10.1007/s00202-012-0275-1.

[4] M. A. Hamdan, A. H. Al Assaf, M. A. Al-Nimr, "Effect of Transverse Steady Magnetic Field on MHD Flow Under Free Convection Conditions in Vertical Microchannels", Jordan Journal of Mechanical and Industrial Engineering, vol. 12, no. 2, 2018, pp. 131–139. https://jjmie.hu.edu.jo/vol12-2/JJMIE-62-17-01.pdf.

[5] B. S. Malga, N. Kishan, V. V Reddy, K. Govardhan, "Finite Element Analysis of Fully Developed Free Convection Flow Heat and Mass Transfer of a MHD / Micropolar Fluid over a Vertical Channel",Jordan Journal of Mechanical and Industrial Engineering, vol. 8, no. 4, 2014, pp. 219–232. https://jjmie.hu.edu.jo/vol%208-4/JJMIE-16-13-01.pdf.

[6] H. Teimouri, A. Behzadmehr, "Numerical investigation of a thermosyphon MHD electrical power generator", Energy Conversion and Management, vol. 187, 2019, pp. 378–397. https://doi.org/10.1016/j.enconman.2019.02.085.

[7] E. Sawaya, N. Ghaddar, F. Chaaban, "Evaluation of the Hall parameter of electrolyte solutions in thermosyphonic MHD flow", International Journal of Engineering Science, vol. 40, no. 18, 2020, pp. 2041–2056. https://doi.org/10.1016/S0020-7225(02)00108-8.

[8] P. Satyamurthy, T. K. Thiyagarajan, N. Venkatramani, "A conceptual scheme for electrical power generation from nuclear waste heat using liquid metal magnetohydrodynamic energy converter", Energy Conversion and Management, vol. 36, no. 10, 1995, pp. 975–987. https://doi.org/10.1016/0196-8904(94)00082-B.

[9] D. Ryan, C. Loescher, I. Hamilton, R. Bean, A. Dix, "Magnetic variation and power density of gravity driven liquid metal magnetohydrodynamic generators", Annals of Nuclear Energy, vol. 114, 2018, pp. 325–328. https://doi.org/10.1016/j.anucene.2017.12.047.

[10] O.M. Al-Habahbeh, M. Al-Saqqa, M. Safi, T. Abo Khater, "Review of magnetohydrodynamic pump applications", Alexandria Engineering Journal, vol. 55, no. 2, 2016, pp. 1347–1358. https://doi.org/10.1016/j.aej.2016.03.001.

[11] P. Satyamurthy, N. Venkatramani, A. M. Quraishi, A. Mushtaq, "Basic design of a prototype liquid metal magnetohydrodynamic power generator for solar and waste heat", Energy Conversion and Management, vol. 40, no. 9, 1999, pp. 913–935. https://doi.org/10.1016/S0196-8904(98)00154-X.

[12] D. Saphier, "Dynamic simulation of a magnetohydrodynamic liquid-metal direct-current generator", Mathematics and Computers in Simulation, vol. 20, no. 1, 1978, pp. 10–17. https://doi.org/10.1016/0378-4754(78)90049-6.

[13] X. Liu, T. Kiyoshi, M. Takeda, "Simulation of a seawater MHD power generation system" Cryogenics, vol. 46, no. 5, 2006, pp. 362–366. https://doi.org/10.1016/j.cryogenics.2005.10.016.

[14] A. Brekis, A. Alemany, J. Freibergs, "Analysis of magnetohydrodynamic generator driven by thermoacoustic engine for deep Space applications", IEEE 61st International Scientific Conference on Power and Electrical Engineering of Riga Technical University, Riga, Latvia, 2020. http://dx.doi.org/10.1109/RTUCON51174.2020.9316584.

[15] T. Alam, M. Kim, "A comprehensive review on single phase heat transfer enhancement techniques in heat exchanger applications", Renewable and Sustainable Energy Reviews, vol. 81, 2017, pp. 813–839. https://doi.org/10.1016/j.rser.2017.08.060.

[16] U. S. Rajput, G. Kumar, "Chemical reaction effect on unsteady MHD flow past an impulsively started inclined plate with variable temperature and mass diffusion in the presence of hall current", Jordan Journal of Mechanical and Industrial Engineering, vol. 11, no. 1, 2017, pp. 41–49. https://jjmie.hu.edu.jo/vol%2011-1/JJMIE-13-16-01.pdf.

[17] I. Shravani, D. Ramya, S. Joga, "MHD tangent hyperbolic nanofluid with zero normal flux of nanoparticles at the stretching surface with thermal radiation", Jordan Journal of Mechanical and Industrial Engineering, vol. 12, no. 3, 2018, pp. 171–177.https://jjmie.hu.edu.jo/vol12-3/JJMIE-66-18-01.pdf.

[18] K. Singh, M. Kumar, "Melting heat transfer in boundary layer stagnation point flow of MHD micro-polar fluid towards a stretching / shrinking surface", Jordan Journal of Mechanical and Industrial Engineering, vol. 8, no. 6, 2014, pp. 403–408.https://jjmie.hu.edu.jo/vol%208-6/JJMIE-77-14-01%20Proof%20OK!.pdf.

[19] K. Singh, M. Kumar, "The effect of chemical reaction and double stratification on MHD free convection in a micropolar fluid with heat generation and ohmic heating", Jordan Journal of Mechanical and Industrial Engineering, vol. 9, no.4, 2015, pp. 279–288.https://jjmie.hu.edu.jo/vol9-4/JJMIE-12-15-01%20Proof%20Reading%20ok.pdf.

[20] Z. Uddin, M. Kumari, "MHD heat and mass transfer free convection flow near the lower stagnation point of an isothermal cylinder imbedded in porous domain with the presence of radiation", JJMIE, vol. 5, no. 5, 2011, pp. 419–423.https://jjmie.hu.edu.jo/files/v5n5/JJMIE-163-09.pdf.

[21] Z. Uddin, M. Kumar, "Mhd heat and mass transfer free convection flow near the lower stagnation point of an isothermal cylinder imbedded in porous domain with the presence of radiation", Jordan Journal of Mechanical and Industrial Engineering, vol. 5, no. 2, 2011, pp. 133–138.https://jjmie.hu.edu.jo/files/v5n2/JJMIE-165-09%20%20(india)(4).pdf.

[22] M. Shareef, "MHD flow along a vertical plate with heat and mass transfer under ramped plate temperature", Jordan Journal of Mechanical and Industrial Engineering, vol. 17, no. 2, 2023, pp. 183–193.https://jjmie.hu.edu.jo/vol17/vol17-2/03-JJMIE-134-23.pdf.

[23] S. R. Kumar, "The effect of the couple stress fluid flow on MHD peristaltic motion with uniform porous medium in the presence of slip effect", Jordan Journal of Mechanical and Industrial Engineering, vol. 9, no.4, 2015, pp. 269–278.https://jjmie.hu.edu.jo/vol9-4/JJMIE-27-15-01.pdf.

[24] M. Wang, H. Zhao, Y. Zhang, G. Su, W. Tian, S. Qiu, "Research on the designed emergency passive residual heat removal system during the station blackout scenario for CPR1000", Annals of Nuclear Energy, vol. 45, 2012, pp. 86–93. https://doi.org/10.1016/j.anucene.2012.03.004.

[25] Y. K. Joshi, W. Nakayama, "A natural circulation model of the closed-loop, two-phase thermosyphon for electronics cooling," J. Heat Transfer, vol. 124, no. 5, 2002, pp. 86–93. https://doi.org/10.1115/1.1482404.

[26] M. A. Siddiqui, "Heat transfer and fluid flow studies in the collector tubes of a closed-loop natural circulation solar water heater", Energy Conversion and Management, vol. 38, no. 8, 1997, pp. 799–812. https://doi.org/10.1016/S0196-8904(96)00097-0.

[27] H. Cohen, F. J. Bayley, "Heat- transfer problems of liquid-cooled gas- turbine blades", Institution of Mechanical Engineers, vol. 169, no. 1, 1955, pp. 1063–1080. https://doi.org/10.1243/PIME_PROC_1955_169_106_02.

[28] D. B. Kreitlow, G. M. Reistad, C. R. Miles, G. G. Culver, "Thermosyphon models for downhole heat exchanger applications in shallow geothermal systems", J. Heat Transfer, vol. 100, no. 4, 1978, pp. 713–719. https://doi.org/10.1115/1.3450883.

[29] H. Cheng, H. Lei, C. Dai, "Heat transfer of a single-phase natural circulation loop with heating and cooling fluids", Energy Procedia, vol. 142, 2017, pp. 3962–3931. http://dx.doi.org/10.1016/j.egypro.2017.12.298.

[30] H. Cheng, H. Lei, L. Zeng, C. Dai, "Theoretical and experimental studies of heat transfer characteristics of a single-phase natural circulation mini-loop with end heat exchangers", International Journal of Heat and Mass Transfer, vol. 128, 2019, pp. 208–216. https://doi.org/10.1016/j.ijheatmasstransfer.2018.08.136.

[31] D. N. Basu, S. Bhattacharyya, P. K. Das, "Performance comparison of rectangular and toroidal natural circulation loops under steady and transient conditions", International Journal of Thermal Sciences, vol. 57, 2012, pp. 142–151. https://doi.org/10.1016/j.ijthermalsci.2012.02.011.

[32] K. K. Kumar, M. R. Gopal, "Steady-state analysis of CO2 based natural circulation loops with end heat exchangers", Applied Thermal Engineering, vol. 29, no. 10, 2009, pp. 1893–1903. https://doi.org/10.1016/j.applthermaleng.2008.08.002.

[33] R. Saha, S. Sen, S. Mookherjee, K. Ghosh, A. Mukhopadhyay, D. Sanyal, "Experimental and Numerical Investigation of a Single-Phase Square Natural Circulation Loop", J. Heat Transfer, vol. 137, no. 12, 2015, pp. 1–8. https://doi.org/10.1115/1.4030926.

[34] P. K. Vijayan, "Experimental observations on the general trends of the steady state and stability behaviour of single-phase natural circulation loops", Nuclear Engineering and Design, vol. 215, no. 1–2, 2002, pp. 139–152. https://doi.org/10.1016/S0029-5493(02)00047-X.

[35] N. Goudarzi, S. Talebi, "An approach to stability analysis and entropy generation minimization in the single-phase natural circulation loops", Energy, vol. 80, 2015, pp. 213–226. https://doi.org/10.1016/j.energy.2014.11.064.

[36] M. Misale, P. Garibaldi, J. C. Passos, G. G. de Bitencourt, "Experiments in a single-phase natural circulation mini-loop", Experimental Thermal and Fluid Science, vol. 31, no. 8, 2007, pp. 1111–1120. https://doi.org/10.1016/j.expthermflusci.2006.11.004.

[37] S. M. Seyyedi, N. Sahebi, A. S. Dogonchi, M. Hashemi-Tilehnoee, "Numerical and experimental analysis of a rectangular single-phase natural circulation loop with asymmetric heater position", International Journal of Heat and Mass Transfer, vol. 130, 2019, pp. 1343–1357. https://doi.org/10.1016/j.ijheatmasstransfer.2018.11.030.

[38] I. Budihardjo, G. L. Morrison, M. Behnia, "Natural circulation flow through water-in-glass evacuated tube solar collectors", Solar Energy, vol. 81, no. 12, 2007, pp. 1460–1472. https://doi.org/10.1016/j.solener.2007.03.002.

[39] M. Hashemi-Tilehnoee, N. Sahebi, A. S. Dogonchi, S. M. Seyyedi, S. Tashakor, "Simulation of the dynamic behavior of a rectangular single-phase natural circulation vertical loop with asymmetric heater", International Journal of Heat and Mass Transfer, vol. 139, 2019, pp. 974–981. https://doi.org/10.1016/j.ijheatmasstransfer.2019.05.076.

[40] S. K. Mousavian, M. Misale, F. D'Auria, M. A. Salehi, "Transient and stability analysis in single-phase natural circulation", Annals of Nuclear Energy, vol. 31, no. 10, 2004, pp. 1177–1198. https://doi.org/10.1016/j.anucene.2004.01.005.

[41] D. S. Pilkhwal, W. Ambrosini, N. Forgione, P. K. Vijayan, D. Saha, J. C. Ferreri, "Analysis of the unstable behaviour of a single-phase natural circulation loop with one-dimensional and computational fluid-dynamic models", Annals of Nuclear Energy, vol. 34, no. 5, 2007, pp. 339–355. https://doi.org/10.1016/j.anucene.2007.01.012.

[42] P. K. Vijayan, H. Austregesilo, V. Teschendorff, "Simulation of the unstable oscillatory behavior of single-phase natural circulation with repetitive flow reversals in a rectangular loop using the computer code athlete", Nuclear Engineering and Design, vol. 155, no. 3, 1995, pp. 623–641. https://doi.org/10.1016/0029-5493(94)00972-2.

[43] D. C. Montgomery, G. C. Runger. Applied Statistics and Probability for Engineers. 3rd ed. Hoboken: John Wiley & Sons; 1994.

## Appendix

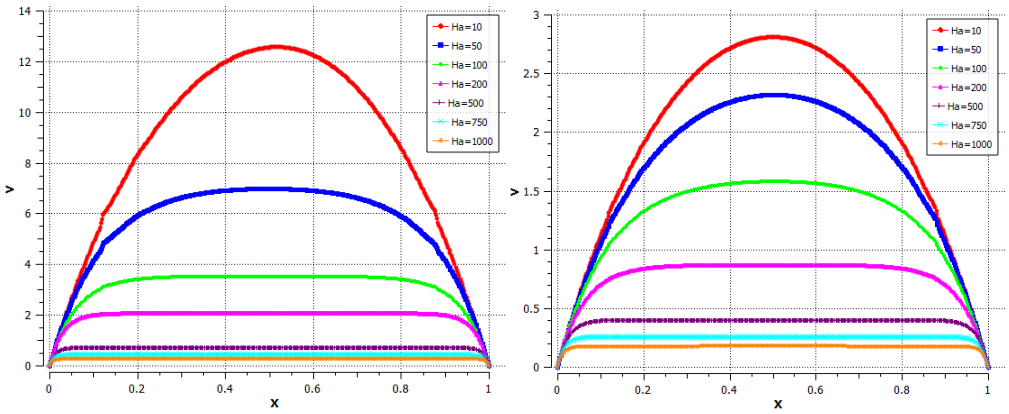


**Figure S1:** The dimensionless vertical velocity profile at the heater section in SPNCl LM MHDG for different Ha at Ar = 6 and 12 and Ra = 1E+04 for Mercury.

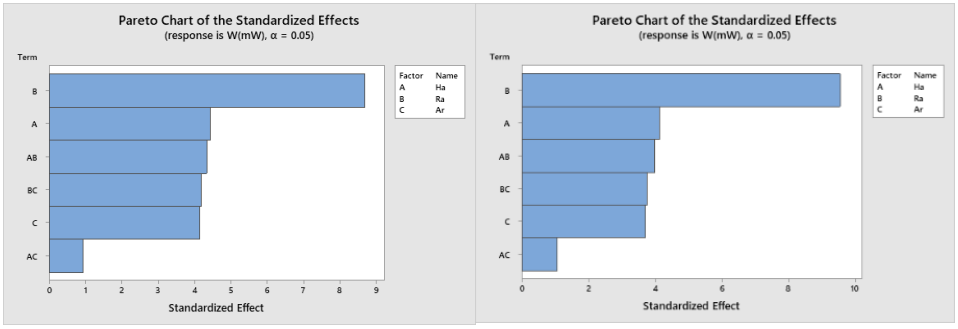


**Mercury** **Gallium**

**Figure S2:** Pareto chart of the standardized effects for (Rayleigh number (Ra) and Hartmann number (Ha)), (response is generated electrical power) for Mercury and Gallium.

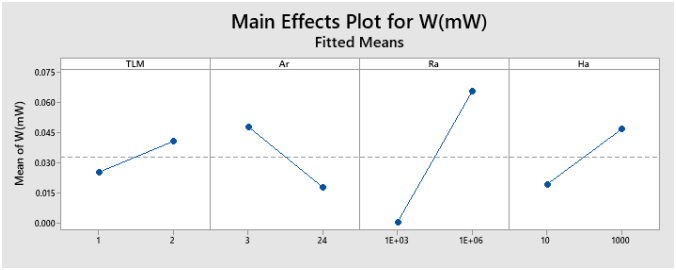


**a.) Main effects plot for generated electrical power.**

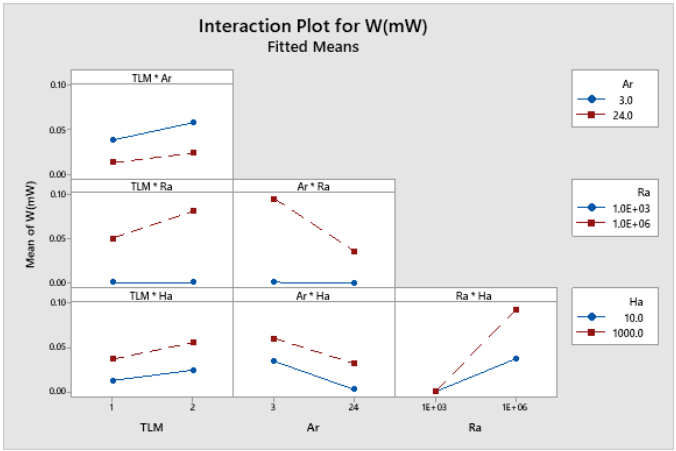


**b.) Interaction plot for generated electrical power.**

**Figure S3:** Main effects and interaction plots for generated electrical power.

 

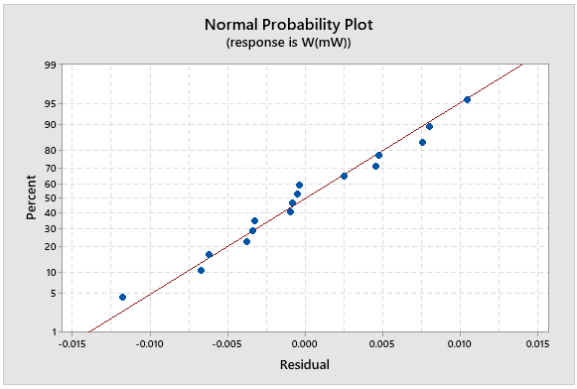


**Figure S4:** Normal probability plot of the residuals for generated electrical power.

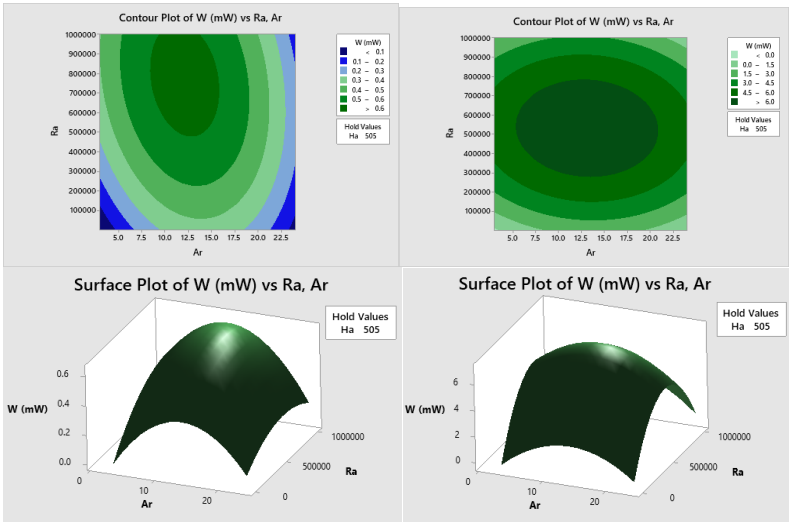


**Mercury** **Gallium**

**Figure S5:** Contour and surface plot of generated electrical power vs Rayleigh number (Ra),Aspect Ratio (Ar) for Mercury and Gallium.

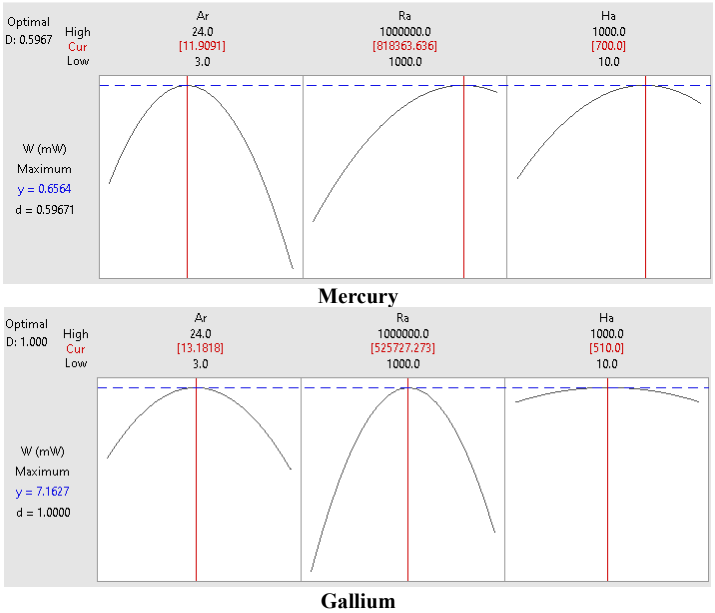


**Mercury**

**Gallium**

**Figure S6:** Optimal design conditionin RSM.